

Available online at [www.sciencedirect.com](http://www.sciencedirect.com)

ScienceDirect

[www.elsevier.com/locate/jes](http://www.elsevier.com/locate/jes)

# Enhancement of photocatalytic efficiency by *in situ* fabrication of BiOBr/BiVO<sub>4</sub> surface junctions

Wenzong Yin, Xiang Sun, Wenzhong Wang\*

State Key Laboratory of High Performance Ceramics and Superfine Microstructure, Shanghai Institute of Ceramics, Chinese Academy of Sciences, Shanghai 200050, China. E-mail: [yinwz@nimte.ac.cn](mailto:yinwz@nimte.ac.cn)

## ARTICLE INFO

### Article history:

Received 28 September 2016

Revised 31 October 2016

Accepted 5 January 2017

Available online 14 March 2017

### Keywords:

Surface junction

Photocatalysis

N-deethylation

Adsorption efficiency

Redox potential

## ABSTRACT

Surface junctions between BiOBr and BiVO<sub>4</sub> were synthesized. The BiOBr/BiVO<sub>4</sub> with 1 wt.% of BiOBr exhibited the highest photocatalytic activity in the degradation of RhB under visible-light irradiation. It was found that the highly efficient adsorption of RhB molecules via the electrostatic attraction between Br<sup>-</sup> and cationic -N(Et)<sub>2</sub> group played a key role for the high photocatalytic activities of BiOBr/BiVO<sub>4</sub>. This efficient adsorption promoted the N-deethylation of RhB and thus accelerated the photocatalytic degradation of RhB. Moreover, the metal-to-metal charge transfer (MMCT) mechanism was proposed, which revealed the concrete path paved with Bi–O–Bi chains for the carrier migration in BiOBr/BiVO<sub>4</sub>. The interaction between photoexcited RhB\* and the Bi<sup>3+</sup> in BiVO<sub>4</sub> provided the driving force for the migration of photo-generated carriers along the Bi–O–Bi chains. This work has not only demonstrated the important role of efficient adsorption in the photocatalytic degradation of organic contaminants, but also developed a facile strategy to improve the efficiency of photocatalysts.

© 2017 The Research Center for Eco-Environmental Sciences, Chinese Academy of Sciences.

Published by Elsevier B.V.

## Introduction

Photocatalytic activity in the degradation of contaminants involves two aspects: photocatalytic ability and photocatalytic efficiency. Once a photocatalyst possesses the ability to degrade certain contaminant, the work to improve its photocatalytic efficiency is on the agenda. As photocatalytic degradation of contaminants takes place on the surface of the photocatalysts (Fujishima et al., 2008), it is critical for photocatalysts to contact efficiently with the molecules of contaminants so as to enhance the degradation efficiencies. Recently, Han and coworkers (Han et al., 2009) have improved the photocatalytic efficiency of TiO<sub>2</sub> by exposing the high reactive (001) facets of TiO<sub>2</sub>. The (001) facets presents high surface energies and thus exhibits intense adsorption of dye molecules. Wang et al. (2008a), Wang et al. (2008b) have found that the photocatalytic efficiency of TiO<sub>2</sub> was

significantly enhanced by surface fluorination using hydrogen fluoride (HF) solution. This fluorination established the substitution of adsorbed OH<sup>-</sup> with F<sup>-</sup>. The adsorbed F<sup>-</sup> increased both the saturation amount and the adsorption strength for organic dyes via the interaction with the cationic moiety. However, the adsorbed F<sup>-</sup> is not stable enough and can be easily washed away. An alternative strategy is to fabricate surface junctions by loading fluoride or other halides onto the surface of photocatalyst and expose the reactive facets of the halides for active adsorption.

Monoclinic BiVO<sub>4</sub> (*m*-BiVO<sub>4</sub>) exhibited photocatalytic activities in the degradation of rhodamine B (RhB) under visible-light irradiation. However, the degradation rates were not satisfying as expected partially because of the inactive adsorption. Meanwhile, BiOBr with exposed (001) facets showed active adsorption of RhB molecules (An et al., 2008). Therefore, the photocatalytic efficiency of *m*-BiVO<sub>4</sub> is expected to be enhanced by loading

\* Corresponding author. E-mail: [wzwang@mail.sic.ac.cn](mailto:wzwang@mail.sic.ac.cn) (Wenzhong Wang).

appropriate amount of BiOBr on its surface to increase the adsorption of RhB molecules. Herein, BiOBr/BiVO<sub>4</sub> surface junctions were fabricated *in situ* via the reaction between BiOBr and VO<sub>3</sub><sup>-</sup>. The content of BiOBr in the product was tuned by changing the amount of VO<sub>3</sub><sup>-</sup> (Yin et al., 2010). The surface-loaded BiOBr not only enhanced the adsorption of RhB molecules, but also paved a Bi–O–Bi path for the migration of electrons from photoexcited RhB\* to BiVO<sub>4</sub>. Thus, the photocatalytic efficiency of *m*-BiVO<sub>4</sub> in the degradation of RhB was enhanced significantly.

## 1. Experimental

All the reagents (Purchased from Shanghai Chemical Company, China) were of analytical purity and used without further purification. In a typical preparation, 2 mmol of Bi(NO<sub>3</sub>)<sub>3</sub>·5H<sub>2</sub>O was added into de-ionized water under magnetic stirring to form a hydrolyzed white floccule. Meanwhile, appropriate amount of NH<sub>4</sub>VO<sub>3</sub> was dissolved into 20 mL of de-ionized water at 96°C and cooled down to room temperature. The NH<sub>4</sub>VO<sub>3</sub> solution was then added dropwise into 40 mL of cetyltrimethylammonium bromide (CTAB) solution with the concentration of 0.1 mol/L. The floccule suspension of Bi(NO<sub>3</sub>)<sub>3</sub> was added into the mixture of CTAB solution and NH<sub>4</sub>VO<sub>3</sub> solution under stirring. After that, the mixture was heated at 80°C for 12 hr. The final product was centrifuged, washed with de-ionized water and absolute ethanol for several times, and dried in air. This series of composite photocatalysts was denoted as CP-*x*, where *x* is the mass percentage of loaded BiOBr.

The X-ray diffraction (XRD) patterns of the as-prepared samples were measured with a Rigaku D/Max-2200PC (Rigaku, Japan) diffractometer using monochromatized Cu K $\alpha$  radiation ( $\lambda = 0.15418$  nm) at a scanning rate of 8°/min. The diffuse reflectance spectra (DRS) were obtained on a UV–vis spectrophotometer Hitachi U-3010, (Hitachi, Japan) using BaSO<sub>4</sub> as the reference. The conduction band of BiVO<sub>4</sub> and BiOBr was measured via Mott–Scottky method. The Mott–Scottky plots of the as-prepared samples were evaluated by a standard three-electrode configuration using an electrochemical workstation (CHI660E, Shanghai Chenhua, China). 0.5 M of Na<sub>2</sub>SO<sub>4</sub> solution was used as the electrolyte. The working electrode was prepared by depositing photocatalyst powders on 1.0 cm × 1.0 cm fluoride-tin oxide (FTO) glass. A saturated calomel electrode (SCE) and platinum wire counter electrode ( $\Phi$  0.5 mm × 37 mm) were employed as the reference and counter electrodes, respectively. The morphology and microstructure of annealed samples were investigated by transmission electron microscopy (TEM) on a JEOL JEM-2100F (JEOL Ltd., Japan).

The photocatalytic efficiencies of the BiOBr/BiVO<sub>4</sub> were evaluated by the degradation of RhB under visible-light irradiation. The visible-light was provided by a 500 W Xenon lamp with a 420 nm cutoff filter. Each experiment was performed at room temperature as follows: 0.1 g of photocatalyst was added into 100 mL of RhB solution with a concentration of 10<sup>-5</sup> mol/L. Before illumination, the suspension was stirred in the dark for 12 hr to ensure an adsorption/desorption equilibrium between RhB and the photocatalyst. Then the suspension was stirred and exposed to visible-light irradiation. At given time intervals, 2 mL of the suspensions was taken out and centrifuged to remove the

photocatalyst particles. The concentrations of the centrifuged RhB solutions were monitored using a Hitachi U-3010 UV–vis spectrophotometer (Hitachi, Japan). The cycling test of the RhB photodegradation was also performed. Chemical oxygen demand (COD) was estimated before and after the treatment using the K<sub>2</sub>Cr<sub>2</sub>O<sub>7</sub> oxidation method.

## 2. Results and discussion

### 2.1. Phases and photocatalytic activities of the series of CP-*x*

Fig. 1 displays the XRD patterns of the series of CP-*x* (*x* = 0, 1, 2, 4). Only the diffraction peaks of *m*-BiVO<sub>4</sub> (JCPDS no. 14-0688) are found in the patterns when the content of BiOBr is lower than 4%. But as the content reaches 8% (Fig. S1), diffraction peaks of BiOBr (JCPDS cards no. 09-0393) appear. Given the detection limitation of XRD (~5 wt.%), these results confirm the successful preparation of BiOBr/BiVO<sub>4</sub> composite photocatalysts. Moreover, the relative intensity of (001) facets is significantly higher than the standard (Fig. S1), indicating the preferred exposure of (001) facets. This speculation is further confirmed by the XRD pattern of the pure BiOBr crystals prepared under the same conditions (Fig. S2). Fig. S3 shows the microscopic morphology of BiOBr/BiVO<sub>4</sub> under low magnification, from which tetragonal BiOBr is observed being deposited on the surface of BiVO<sub>4</sub>. When the CP-8 was further calcined at 500°C for 2 hr (denoted as CP-8-cal), BiOBr has disappeared (Fig. S4). Instead, Bi<sub>2</sub>VO<sub>5.5</sub> has emerged and the BiOBr/BiVO<sub>4</sub> has transformed into Bi<sub>2</sub>VO<sub>5.5</sub>/BiVO<sub>4</sub>. As the Bi<sub>2</sub>VO<sub>5.5</sub> (or BiVO<sub>4</sub>·0.5Bi<sub>2</sub>O<sub>3</sub>) can be referred as the solid solution of BiVO<sub>4</sub> and Bi<sub>2</sub>O<sub>3</sub>, it is reasonable to speculate following reactions carried out:



Fig. 2 shows the photocatalytic activities of the series of CP-*x* (*x* = 0, 0.5, 1, 2, 4) in the degradation of RhB. The changing

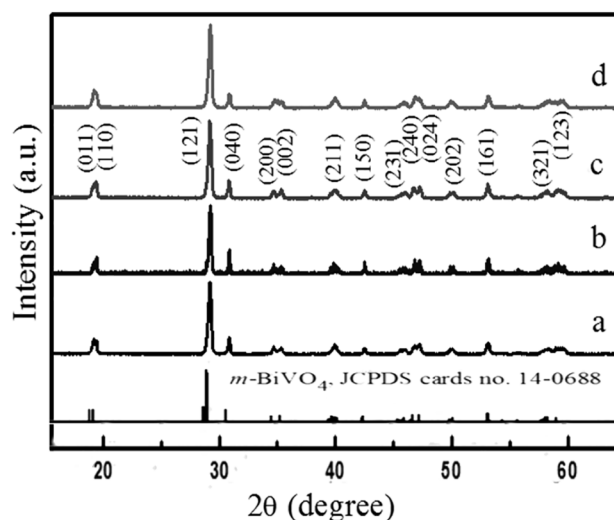


Fig. 1 – XRD patterns of CP-0.5 a, CP-1 b, CP-2 c, and CP-4 d. XRD: X-ray diffraction.

of  $C/C_0$  during the dark equilibrium was also recorded over different samples (Fig. S5). The major absorption band of RhB is centered at 553 nm and used to monitor the concentration of RhB. It is obvious that the photocatalytic efficiency of  $\text{BiVO}_4$  is significantly improved by coupling with BiOBr. When the content of BiOBr is lower than 4%, the CP-1 exhibits the highest degradation efficiency and the perfect stability (Fig. S6). This demonstrates the existence of an optimal content of loaded BiOBr for enhancing the photocatalytic activity of  $\text{BiVO}_4$ . The percentage change of the COD, which reflects the extent of mineralization of an organic species, was studied as a function of irradiation time in the photodegradation of RhB ( $10^{-5}$  mol/L) under visible-light (shown in Fig. S7), in order to further confirm the activity of the photocatalyst from the photocatalysis. If the dye was not degraded completely, the residual organic molecules could be oxidized by  $\text{K}_2\text{Cr}_2\text{O}_7$ , thus the oxygen demand could be more, and the COD would be bigger than that of the completely mineralized dye. The initial COD of the RhB solution is 250.8 mg/L. After visible-light irradiation for 2 hr, the COD decreased markedly to 47.9 mg/L. The significant reduction of COD (81.0%) further confirms that RhB was truly photodegraded by CP-1% sample. Similar results have been widely reported in other composite photocatalysts (Zong et al., 2008; Lu et al., 2008). Since BiOBr also shows good photocatalytic activities under visible-light, the enhanced photocatalytic activities of the CP-1 might be attributed to the introduction of BiOBr. For further investigation, a mechanically mixed sample with 1% of BiOBr and 99% of  $\text{BiVO}_4$  (denoted as MM-1%) was prepared. Its photocatalytic efficiency was evaluated by the degradation of RhB under the same conditions (Fig. 2). Only 33.7% of RhB has been degraded after 60 min of irradiation over the MM-1%. Such low efficiency not only excludes the sole role of the 1% BiOBr on the enhanced photocatalytic efficiency, but also indicates a possible heterostructure formed between BiOBr and  $\text{BiVO}_4$  in CP-1.

## 2.2. Mechanisms for the enhanced photocatalytic efficiency of the CP-1

As reported in Ref. (Hu et al., 2006), RhB dye is zwitterionic and can be degraded in two different pathways: *N*-deethylation and

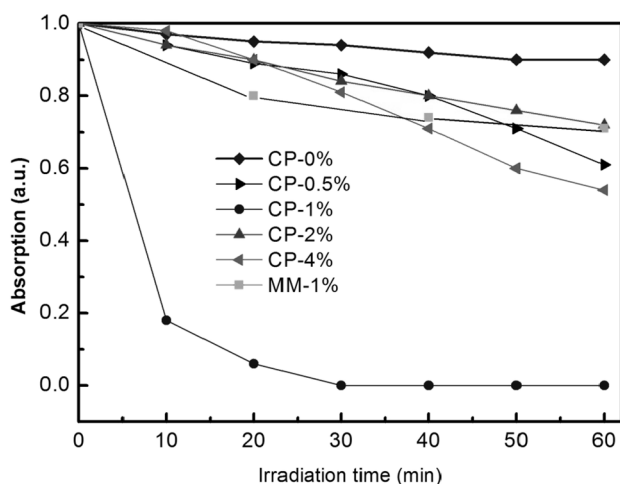


Fig. 2 – Decrease of RhB ( $C/C_0$ ) (100 mL,  $10^{-5}$  mol/L) as a function of irradiation time over 0.1 g different photocatalysts under visible-light ( $\lambda > 420$  nm). RhB: rhodamine B.

direct cleavage of conjugated chromophore structure. The former one can be characterized by the shift of the maximum absorption band ( $\lambda_{\text{max}}$ ) of RhB while the latter one by the change in the absorption maximum ( $A_{\text{max}}/A_{\text{max}}^0$ ). These two procedures usually take place simultaneously in the presence of photocatalyst under irradiation. As a result, it is a cooperative effect that results in the decrease of absorbance at the wavelength of 553 nm with the irradiation time prolonged. Furthermore, Wang and coworkers (Wang et al., 2008a; Wang et al., 2008b) revealed that the two degradation pathways of RhB depended greatly on the adsorption modes of zwitterionic RhB on the surface of photocatalysts. If the adsorption performed via the cationic moiety ( $-\text{N}(\text{Et})_2$  group), *N*-deethylation predominated in the degradation pathways before destruction of the chromophore structure. When adsorbed through the carboxylic ( $-\text{COOH}$ ) group, however, RhB experienced direct cleavage of chromophore structure.

To clarify the degradation pathway of RhB over the CP-1, the hypsochromic shifts of  $\lambda_{\text{max}}$  and the decrease of  $A_{\text{max}}/A_{\text{max}}^0$  were investigated respectively (Fig. 3). After irradiated for 20 min,  $\lambda_{\text{max}}$  shifted from 553 nm to 501 nm. This value is very close to the  $\lambda_{\text{max}}$  (498 nm) of the fully-deethylated RhB (rhodamine), indicating that deethylation was nearly accomplished. In contrast,  $A_{\text{max}}/A_{\text{max}}^0$  decreases by 95% even after 60 min of irradiation. These characteristics are demonstrated in Fig. 4a. The above results reveal that *N*-deethylation has predominated in the degradation of RhB over the CP-1. In this case, it can be speculated that most RhB molecules were adsorbed on the CP-1 via the cationic  $-\text{N}(\text{Et})_2$  moiety. Considering the high electronegativity of  $\text{Br}^-$ , it might be the  $\text{Br}^-$  in BiOBr that facilitates the adsorption. To testify this proposition, the CP-1 was calcined at  $500^\circ\text{C}$  to remove the  $\text{Br}^-$  and the degradation pathway of RhB over the as-prepared CP-1-cal was investigated. The results are shown in Fig. 3. It takes 50 min for  $\lambda_{\text{max}}$  to shift from 553 nm to 501 nm in the degradation over the CP-1-cal while 20 min over the CP-1. In other word, the *N*-deethylation rate over the CP-1 is 2.5 times

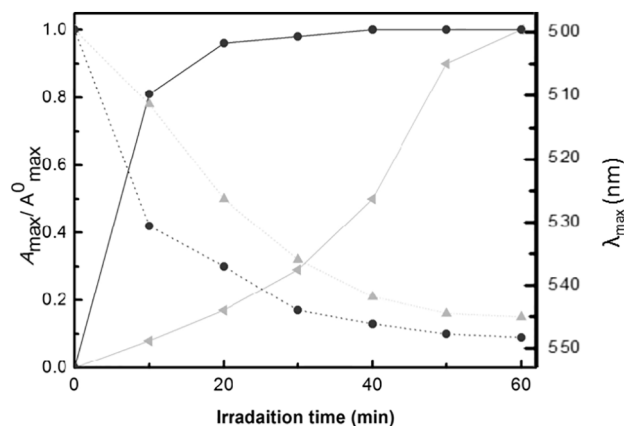


Fig. 3 – Changes of the maximum absorption band ( $\lambda_{\text{max}}$ , dot line) and the absorption maximum ( $A_{\text{max}}/A_{\text{max}}^0$ , solid line) of RhB as a function of irradiation time during the photocatalytic degradation of RhB (100 mL,  $10^{-5}$  mol/L) over CP-1 (0.1 g, circle) and CP-1-cal (0.1 g, triangle).

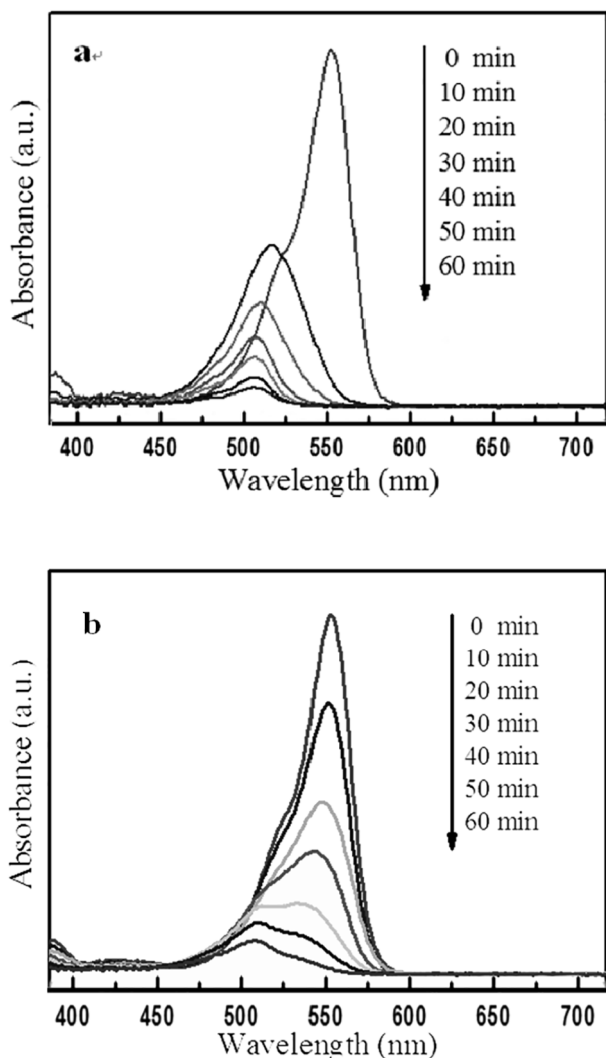


Fig. 4 – UV-Vis spectra of the RhB degraded for different time over CP-1 (a) and CP-1-cal (b) under visible-light irradiation ( $\lambda > 420$  nm).

faster than that over the CP-1-cal. This drastically decline in N-deethylation rate is clearly displayed in Fig. 4b. The rate of the cleavage of conjugated chromophore structure was evaluated with the reaction constant ( $k$ ) determined by the plots of  $\ln(A_{\max}/A_{\max}^0)$  vs irradiation time ( $t$ ). The  $k$  values of the cleavage process are 0.042 and 0.041  $\text{min}^{-1}$  for the degradation over the CP-1 and CP-1-cal, respectively (Fig. S8). Their linearly dependent coefficients ( $R$ ) are 0.997 and 0.995, respectively, suggesting a good linear dependence relation. The neglectable difference between the  $k$  values implies the nearly same rates in cleavage of conjugated chromophore structure. The dramatically dropped N-deethylation rate and the remained cleavage rate of the CP-1-cal reveal that the adsorption of RhB via the cationic  $-\text{N}(\text{Et})_2$  group has declined significantly. Given the substitution of BiOBr with  $\text{Bi}_2\text{VO}_{5.5}$  after calcinations, such decline demonstrates the critical role of  $\text{Br}^-$  in the efficient adsorption of the cationic  $-\text{N}(\text{Et})_2$  moiety of RhB (Fig. 5).

### 2.3. Paths for the migration of photo-generated carriers in the CP-1

The N-deethylation processes during the photocatalytic degradation of RhB are carried out as follows (Hu et al., 2006; Watanabe et al., 1977):



Among the three steps, Reaction (4) is critical for the photocatalytic degradation because it involves the interaction between excited RhB\* and photocatalysts. To clarify the interaction process, we investigated the generation, transfer and release of the photo-generated holes.

Here, the photo-generated holes have two possible sources: BiOBr and  $\text{BiVO}_4$ . As the MM-1 and CP-2 both exhibit far lower degradation rates than the CP-1, it could exclude the BiOBr as the source of the photo-generated holes. Alternatively, these holes should originate predominantly from  $\text{BiVO}_4$ .

Since the excited RhB\* molecules were adsorbed on BiOBr, it is necessary to clarify the way in which the photo-generated holes on  $\text{BiVO}_4$  surface migrate to interact with the excited RhB\* molecules. Concretely, it involves two issues: (1) the origination of the driving force for the carrier migration and (2) the path paved for the migration of photo-generated carrier.

The first issue could be addressed from the viewpoint of photoelectrochemistry. When irradiated by visible-light, RhB was excited into RhB\* and the redox potential ( $\phi$ ) of RhB\* is  $-1.09$  V vs. NHE (Hu et al., 2006). Meanwhile, holes are generated in the VB of the  $\text{BiVO}_4$ . The  $\phi$  value of these holes is the same 2.68 V (vs. NHE) as that of the VB (Fujishima et al., 2000), which is more positive than the 2.0 V of  $\phi$  ( $\text{Bi}^{5+}/\text{Bi}^{3+}$ ) (Qin and Wang, 2000). As a result,  $\text{Bi}^{3+}$  in the surface  $\text{BiVO}_4$  could be oxidized into  $\text{Bi}^{5+}$  by the photoinduced holes. In this case, an electric field with the potential of 3.09 V is set up between the RhB\* and  $\text{Bi}^{5+}$ . With this potential, electrons

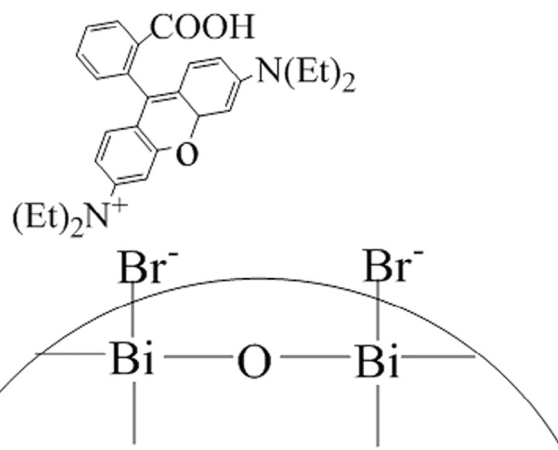
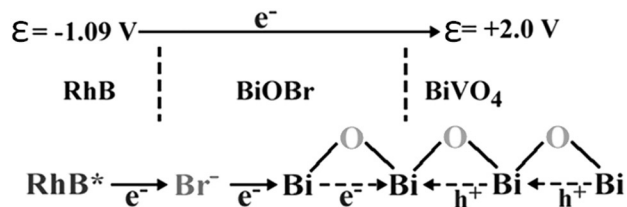


Fig. 5 – Illustration of the adsorption of RhB molecule via cationic  $-\text{N}(\text{Et})_2$  moiety on the surface of BiOBr.



**Scheme 1** – Schematic illustration of the migration of photoinduced carriers in the CP-1 with RhB molecule adsorbed on its surface.

could be driven to migrate from RhB\* to Bi<sup>5+</sup> and holes from Bi<sup>5+</sup> to RhB\* (Scheme 1). Nevertheless, the latter migration could not work out from the viewpoint of heterojunction.

According to semiconductor theory, the heterojunctions can set up a built-in electric field at the interface and thus promote the separation of photo-generated electron-hole pairs (Long et al., 2006; Zhang et al., 2009). The positions of conduction band (CB) and valence band (VB) for monoclinic BiVO<sub>4</sub> and BiOBr have been calculated according to the method in Ref. (Wang et al., 2008a; Wang et al., 2008b). The CB of BiOBr (−0.26 eV) is positioned higher than that of BiVO<sub>4</sub> (0.35 eV) before the two crystals are coupled. But the VB of BiOBr (2.46 eV) is lower than that of BiVO<sub>4</sub> (2.77 eV). The Fermi levels of the two crystals lie at about the middle of their respective band gap (Sun et al., 2003). When BiVO<sub>4</sub> is coupled with BiOBr and the heterojunctions reach a thermodynamic equilibrium, their Fermi levels line up. The renewed energy band positions are displayed in Fig. 6. The CB potentials of BiOBr are more negative than that of BiVO<sub>4</sub>. As a result, a built-in electric field which facilitates the separation of photo-generated carriers is formed at the interface between BiVO<sub>4</sub> and BiOBr (Fig. 6). Hereby, the N-deethylation of RhB could be ascribed to the migration of electrons through bridged BiOBr from RhB\* to BiVO<sub>4</sub>, rather than hole transfer from BiVO<sub>4</sub> to RhB\*.

Although the above discussion verifies that the potential between RhB\* and BiVO<sub>4</sub> works as the driving force for the

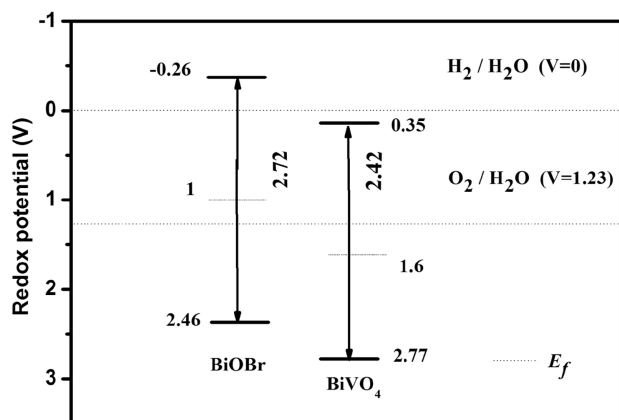
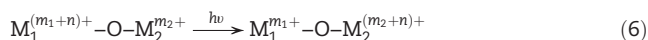


**Fig. 6** – Redox potentials (vs. NHE) for the conduction bands and valence bands of BiOBr and BiVO<sub>4</sub>. NHE: normal hydrogen electrode.

migration of photoinduced carriers, it does not depict the concrete path for carrier migration and what the path paved with. Recently, the metal-to-metal charge transfer (MMCT) theory has been proposed (Lin and Frei, 2005a, 2005b) and developed for the preparation of oxo-bridged hetero-bimetallic complex with photocatalytic activities under visible-light (Nakamura et al., 2007; Nakamura and Frei, 2006). This theory has also found applications in explanation of the photocatalytic activities for Fe-doped SrTiO<sub>3</sub> (Xie et al., 2008), Cr<sup>III</sup>-grafted TiO<sub>2</sub> (Irie et al., 2008), coupled CuO–TiO<sub>2</sub> nanocomposites (Li et al., 2008) and SrTi<sub>1-x</sub>Mn<sub>x</sub>O<sub>3</sub> solid solutions (Sun and Lin, 2009). The photocatalytic reactions involved in the MMCT theory can be generally described as:



where, M<sub>1</sub> and M<sub>2</sub> are two metal ions with variable valence and matched redox potentials, m<sub>1</sub>, m<sub>2</sub> and n are integers depicting the metal valence, O is oxygen element, dash represents the bond between oxygen and metals, hν is the energy of photons from the incident light. When photocatalysts were excited by visible-light, Reaction (6) took place and metal M<sub>2</sub> was oxidized by M<sub>1</sub>. The oxidized M<sub>2</sub> could further oxidize degradable organics. Thus, photo-generated holes are transferred from M<sub>1</sub> to M<sub>2</sub> and then to the organics. Analogically, the transfer of photo-generated carriers during the degradation of RhB over the CP-1 can be explained as follows presuming M<sub>1</sub> = M<sub>2</sub> = Bi.

As a typical bismuth oxyhalide, BiOBr is of matlockite structure. This structure can be characterized by [Bi<sub>2</sub>O<sub>2</sub>] slabs interleaved with double slabs of bromine atoms (Zhang et al., 2008a; Zhang et al., 2008b). In [Bi<sub>2</sub>O<sub>2</sub>] slabs, Bi<sup>3+</sup> ions are bridged through oxygen atoms and thus form Bi–O–Bi chains (Scheme 1). BiVO<sub>4</sub> crystals are perovskite-structured and composed of V–O tetrahedra and Bi–O octahedral (Walsh et al., 2009). The Bi–O octahedra link through corners (O) and the hybridization of Bi 6s and O 2p in BiVO<sub>4</sub> forms a largely delocalized VB that promotes the transfer of photo-generated holes via the Bi–O–Bi path (Oshikiri et al., 2002). Since BiVO<sub>4</sub> was derived from BiOBr, the Bi–O–Bi chains could match well with the Bi–O octahedra on BiVO<sub>4</sub> surface. This match paves the Bi–O–Bi path for photoinduced carriers to transfer from RhB\* to BiVO<sub>4</sub> or vice versa. When irradiated by visible-light, Bi<sup>5+</sup> could be derived via the oxidation of Bi<sup>3+</sup> by photo-generated holes. Meanwhile, RhB was excited into RhB\* and efficiently adsorbed on the surface of BiOBr via the electrostatic attraction between Br<sup>−</sup> and cationic −N(Et)<sub>2</sub> group. The potential between Bi<sup>5+</sup> and RhB\* provided the driving force for the carrier transfer. The electrons could transfer across BiOBr from RhB\* to BiVO<sub>4</sub> via the Bi–O–Bi chains (Scheme 1). The built-in electric field at the interface between BiVO<sub>4</sub> and BiOBr also facilitates this electron transfer. However, the electric field prohibits the holes on BiVO<sub>4</sub> surface to migrate through the interface. Hence, photoinduced holes could only transfer on BiVO<sub>4</sub> surface. In other words, the photoinduced electrons from RhB\* could react with the holes from BiVO<sub>4</sub> either at the interface or on the surface of BiVO<sub>4</sub>, which results in the N-deethylation of RhB.

### 3. Conclusions

BiOBr/BiVO<sub>4</sub> surface junctions were *in situ* fabricated by co-synthesis method. The CP-1 exhibited the highest activities when the content of BiOBr was lower than 4%. The loaded BiOBr on BiVO<sub>4</sub> surface efficiently adsorbed the RhB molecules via the electrostatic attraction between Br<sup>-</sup> and cationic -N(Et)<sub>2</sub> group. This efficient adsorption promoted the N-deethylation of RhB and thus accelerated the photocatalytic degradation of RhB. The potential of ca. 3.09 V between RhB\* and Bi<sup>3+</sup> provided the driving force for the migration of photoinduced carriers in BiOBr/BiVO<sub>4</sub>. Furthermore, the Bi–O–Bi chains in BiOBr/BiVO<sub>4</sub> paved the concrete path for the carrier migration.

### Acknowledgments

This work was supported by National Basic Research Program (973) of China (No. 2013CB933200), the National Natural Science Foundation of China (Nos. 21671197, 51472260), and the Research Grant (No. 16ZR1440800) from Shanghai Science and Technology Commission.

### Appendix A. Supplementary data

Supplementary data to this article can be found online at <http://dx.doi.org/10.1016/j.jes.2016.12.024>.

### REFERENCES

- An, H., Du, Y., Wang, T., Wang, C., Hao, W., Zhang, J., 2008. Photocatalytic properties of BiOX (X = Cl, Br, and I). *Rare Metals* 27, 243–250.
- Fujishima, A., Rao, T., Tryk, D., 2000. Titanium dioxide photocatalysis. *J. Photochem. Photobiol. C* 1, 1–21.
- Fujishima, A., Zhang, X., Tryk, D., 2008. TiO<sub>2</sub> photocatalysis and related surface phenomena. *Surf. Sci. Rep.* 63, 515–582.
- Han, X., Kuang, Q., Jin, M., Xie, Z., Zheng, L., 2009. Synthesis of titania nanosheets with a high percentage of exposed (001) facets and related photocatalytic properties. *J. Am. Chem. Soc.* 131, 3152–3153.
- Hu, X., Mohamood, T., Ma, W., Chen, C., Zhao, J., 2006. Oxidative decomposition of rhodamine B dye in the presence of VO<sub>2</sub><sup>+</sup> and/or Pt(IV) under visible light irradiation: N-deethylation, chromophore cleavage, and mineralization. *J. Phys. Chem. B* 110, 26012–26018.
- Irie, H., Miura, S., Nakamura, R., Hashimoto, K., 2008. A novel visible-light-sensitive efficient photocatalyst, Cr-III-grafted TiO<sub>2</sub>. *Chem. Lett.* 37, 252–253.
- Li, G., Dimitrijevic, N., Chen, L., Rajh, T., Gray, K., 2008. Role of surface/interfacial Cu<sup>2+</sup> sites in the photocatalytic activity of coupled CuO-TiO<sub>2</sub> nanocomposites. *J. Phys. Chem. C* 112, 19040–19044.
- Lin, W., Frei, H., 2005a. Anchored metal-to-metal charge-transfer chromophores in a mesoporous silicate sieve for visible-light activation of titanium centers. *J. Phys. Chem. B* 109, 4929–4935.
- Lin, W., Frei, H., 2005b. Photochemical CO<sub>2</sub> splitting by metal-to-metal charge-transfer excitation in mesoporous ZrCu(I)-MCM-41 silicate sieve. *J. Am. Chem. Soc.* 127, 1610–1611.
- Long, M., Cai, W., Cai, J., Zhou, B., Chai, X., Wu, Y., 2006. Efficient photocatalytic degradation of phenol over Co<sub>3</sub>O<sub>4</sub>/BiVO<sub>4</sub> composite under visible light irradiation. *J. Phys. Chem. B* 110, 20211–20216.
- Lu, W., Gao, S., Wang, J., 2008. One-pot synthesis of Ag/ZnO self-assembled 3D hollow microspheres with enhanced photocatalytic performance. *J. Phys. Chem. C* 112, 16792–16800.
- Nakamura, R., Frei, H., 2006. Visible light-driven water oxidation by Ir oxide clusters coupled to single Cr centers in mesoporous silica. *J. Am. Chem. Soc.* 128, 10668–10669.
- Nakamura, R., Okamoto, A., Osawa, H., Irie, H., Hashimoto, K., 2007. Design of all-inorganic molecular-based photocatalysts sensitive to visible light: Ti(IV)-O-Ce(III) bimetallic assemblies on mesoporous silica. *J. Am. Chem. Soc.* 129, 9596–9597.
- Oshikiri, M., Boero, M., Ye, J., Zou, Z., Kido, G., 2002. Electronic structures of promising photocatalysts InMO<sub>4</sub> (M = V, Nb, Ta) and BiVO<sub>4</sub> for water decomposition in the visible wavelength region. *J. Chem. Phys.* 117, 7313–7318.
- Qin, Y., Wang, Y., 2000. Thermodynamic equilibrium of Bi<sup>3+</sup>-Cl<sup>-</sup>-H<sub>2</sub>O system. *Chin. J. Nonferrous Met.* 2000 (10), 245–249.
- Sun, X., Lin, J., 2009. Synergetic effects of thermal and photo-catalysis in purification of dye water over SrTi<sub>1-x</sub>Mn<sub>x</sub>O<sub>3</sub> solid solutions. *J. Phys. Chem. C* 113, 4970–4975.
- Sun, B., Vorontsov, A., Smimiotis, P., 2003. Role of platinum deposited on TiO<sub>2</sub> in phenol photocatalytic oxidation. *Langmuir* 19, 3151–3156.
- Walsh, A., Yan, Y., Huda, M., Al-Jassim, M., Wei, S., 2009. Band edge electronic structure of BiVO<sub>4</sub>: elucidating the role of the Bi s and V d orbital. *Chem. Mater.* 21, 547–551.
- Wang, Q., Chen, C., Zhao, D., Ma, W., Zhao, J., 2008a. Change of adsorption modes of dyes on fluorinated TiO<sub>2</sub> and its effect on photocatalytic degradation of dyes under visible irradiation. *Langmuir* 24, 7338–7345.
- Wang, P., Huang, B., Zhang, X., Qin, X., Hao, Y., Wei, J., Whangbo, M., 2008b. Composite semiconductor H<sub>2</sub>WO<sub>4</sub>·H<sub>2</sub>O/AgCl as an efficient and stable photocatalyst under visible light. *Chem. Eur. J.* 14, 10543–10546.
- Watanabe, T., Takizawa, T., Honda, K., 1977. Photo-catalysis through excitation of adsorbates. 1. Highly efficient N-deethylation of rhodamine B adsorbed to CdS. *J. Phys. Chem.* 81, 1845–1851.
- Xie, T., Sun, X., Lin, J., 2008. Enhanced photocatalytic degradation of RhB driven by visible light-induced MMCT of Ti(IV)-O-Fe(II) formed in Fe-doped SrTiO<sub>3</sub>. *J. Phys. Chem. C* 112, 9753–9759.
- Yin, W., Wang, W., Zhou, L., Sun, S., Zhang, L., 2010. CTAB-assisted synthesis of monoclinic BiVO<sub>4</sub> photocatalyst and its highly efficient degradation of organic dye under visible-light irradiation. *J. Hazard. Mater.* 173, 194–199.
- Zhang, J., Xu, Q., Feng, Z., Li, M., Li, C., 2008a. Importance of the relationship between surface phases and photocatalytic activity of TiO<sub>2</sub>. *Angew. Chem. Int. Ed.* 47, 1766–1769.
- Zhang, X., Ai, Z., Jia, F., Zhang, L., 2008b. Generalized one-pot synthesis, characterization, and photocatalytic activity of hierarchical BiOX (X = Cl, Br, I) nanoplate microspheres. *J. Phys. Chem. C* 112, 747–753.
- Zhang, X., Zhang, L., Xie, T., Wang, D., 2009. Low-temperature synthesis and high visible-light-induced photocatalytic activity of BiOI/TiO<sub>2</sub> heterostructures. *J. Phys. Chem. C* 113, 7371–7378.
- Zong, X., Yan, H., Wu, G., Ma, G., Wen, F., Wang, L., Li, C., 2008. Enhancement of photocatalytic H<sub>2</sub> evolution on CdS by loading MoS<sub>2</sub> as cocatalyst under visible light irradiation. *J. Am. Chem. Soc.* 130, 7176–7177.